



New Mo(II) complexes in MCM-41 and silica: Synthesis and catalysis



Marta S. Saraiva^a, Cristina I. Fernandes^a, Teresa G. Nunes^b, Carla D. Nunes^a,
Maria José Calhorda^{a,*}

^aDepartamento de Química e Bioquímica, CQB, Faculdade de Ciências da Universidade de Lisboa, Campo Grande, Ed. C8, 1749-016 Lisboa, Portugal

^bCentro de Química Estrutural, Instituto Superior Técnico, Universidade Técnica de Lisboa, Av. Rovisco Pais, 1049-001 Lisboa, Portugal

ARTICLE INFO

Article history:

Received 30 May 2013

Received in revised form

30 July 2013

Accepted 31 July 2013

Keywords:

Molybdenum complexes

N,O-ligands

MCM-41

Silica

Catalysis

Oxidation

ABSTRACT

The new complexes $[\text{Mo}_2(\text{CO})_3(\text{L}_1)]$ (**1**) and $[\text{Mo}_2(\text{CO})_3(\text{L}_2)]$ (**2**) were prepared from reaction of $[\text{Mo}_2(\text{CO})_3(\text{NCMe})_2]$ with the ligands 2-(2'-hydroxyphenyl)imidazoline (**L**₁), and 2-(2'-hydroxyphenyl)benzimidazole (**L**₂). These complexes were immobilized in MCM-41 and in silica gel, by grafting (3-chloropropyl)trimethylsilane on the surface of the materials and allowing it to react with $[\text{Mo}_2(\text{CO})_3(\text{L}_1)]$ (**1**) or $[\text{Mo}_2(\text{CO})_3(\text{L}_2)]$ (**2**). All the molybdenum derivatives were characterized by NMR and FTIR spectroscopies, which showed coordination of **L**₁ and **L**₂ in neutral form. The structure of the MCM materials was analyzed by powder X-ray diffraction and nitrogen adsorption isotherms. The catalytic activity of the complexes and materials was tested in several substrates (*cis*-cyclooctene, styrene, 1-octene, *R*-(+)-limonene, geraniol, *cis*-hex-3-en-1-ol and *trans*-hex-2-en-1-ol), using *tert*-butylhydroperoxide (TBHP) as oxidant. Complexes **1** and **2** were in general the more active catalysts and 100% selective towards the epoxide of *cis*-cyclooctene. Complex **1** immobilized in silica (**Si-Pr-1**) was the best material, showing higher conversion than **1** in the oxidation of *R*-(+)-limonene, with comparable selectivity towards the ring epoxide.

© 2013 Elsevier B.V. All rights reserved.

1. Introduction

Catalytic processes play a fundamental role in chemical and pharmaceutical industry, making available synthetic routes otherwise impossible. On the other hand, while very selective and active homogeneous catalysts have been developed, it is often difficult to separate the products and to recover the catalyst for reuse. This difficulty is overcome by heterogeneous catalysts, which in general allow an easy separation of products and catalyst [1,2]. The challenge lies in improving the selectivity and other properties of heterogeneous catalysts, so that they may compete with the homogeneous ones. In order to achieve this aim, one possible approach consists in immobilizing homogeneous catalysts in appropriate supports. Unfortunately, in many attempts, the new heterogeneous catalysts do not keep the selectivity associated with the homogeneous conditions. The nature of the support may be important. MCM type materials, initially developed by Mobil Corporation in 1992 [3,4], display promising properties, such as an ordered structure with one-dimensional channels of silicon oxide

with surface silanol groups. The diameter of the pores and the presence of the SiOH groups make further functionalization relatively easy, thus allowing the formation of strong covalent bonds with molecules, organic or inorganic, carrying appropriate substituents. A strong bond between support and catalyst is one requirement to avoid lexiviation of the catalyst when in operation [5–9]. Many examples of functionalized MCM-41 are known, namely in catalysis and materials [1,5,10–12].

In previous works, we described the introduction of Mo(II) complexes in MCM-41, obtaining materials that have proved to be active catalyst precursors for the epoxidation of olefins and in some cases with higher activity than the homogeneous counterparts [9]. However, this behavior is not always observed and sometimes the immobilization damages the catalytic activity of a particular metal center [7,13–15]. The effect of each factor cannot yet be totally rationalized, so that it is still relevant to examine new systems. In the family of $[\text{MoX}_2(\text{CO})_3(\text{NCMe})_2]$ complexes [16], the NCMe ligands have been substituted by a variety of nitrogen bidentate ligands (N–N), while X has been I or Br [9,17]. Catalysts with X = I are usually more active in epoxidation reactions than the Br analogues. The N–N ligands are prepared for grafting in the MCM-41 material by carrying a $-\text{Si}(\text{OR})_3$ group, or another function, such as NH which can be attached to a suitable spacer. The nature and size of the spacer may also be varied to a certain extent.

* Corresponding author. Tel.: +351 217500196; fax: +351 217500088.

E-mail addresses: mssaraiva@fc.ul.pt (M.S. Saraiva), cifernandes@fc.ul.pt (C.I. Fernandes), teresa.nunes@ist.utl.pt (T.G. Nunes), cmnunes@fc.ul.pt (C.D. Nunes), mjc@fc.ul.pt (M.J. Calhorda).

Molybdenum compounds have been known as catalysts for olefin epoxidation, being used in the ARCO-Halcon process for homogeneous olefin epoxidation with TBHP as oxidant [18]. Many other systems were developed containing either Mo(VI) [19,20] or a Mo(II) precursor [21], and many showed a high activity in the same kind of reaction or others [22–25]. More recently, chiral molybdenum catalysts have been immobilized in MCM-41 in order to improve enantioselective oxidation. [26,27]

In this work, the two ligands chosen bind the metal in a κ^2 -N,O mode, so that the effect of a mixed N,O donor in the catalytic activity of two new Mo(II) complexes can be studied. Besides, plain silica and MCM-41 were tested and compared as supports, since silica is easily available and much cheaper. The type of support has been shown to modify the catalytic activity of Mo(II) complexes [28].

2. Results and discussion

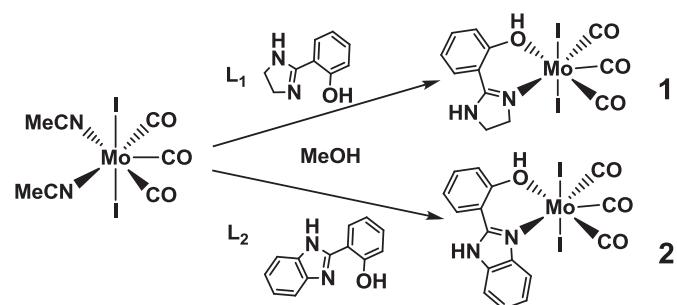
2.1. Synthesis and characterization of complexes

The new complexes $[\text{Mo}_2(\text{CO})_3(\text{L}_1)]$ (**1**) and $[\text{Mo}_2(\text{CO})_3(\text{L}_2)]$ (**2**) were prepared by adding a solution of the ligand, 2-(2'-hydroxyphenyl)imidazole (**L**₁) or 2-(2'-hydroxyphenyl)benzimidazole (**L**₂), respectively [29–31], to $[\text{Mo}_2(\text{CO})_3(\text{NCMe})_2]$ [16], in methanol, overnight (Scheme 1).

They were characterized by elemental analysis, FTIR, and ¹H and ¹³C NMR spectroscopy. The two ligands usually coordinate the metal in an anionic form, having lost the H(O) proton during the complexation reaction [32]. Spectroscopic data showed that this did not happen in the reaction with $[\text{Mo}_2(\text{CO})_3(\text{NCMe})_2]$, the ligands remaining neutral and protonated.

The signals in the ¹H and ¹³C NMR spectra of complexes $[\text{Mo}_2(\text{CO})_3(\text{L}_1)]$ (**1**) and $[\text{Mo}_2(\text{CO})_3(\text{L}_2)]$ (**2**) in DMSO-*d*⁶ solution were assigned with the help of COSY and HMQC experiments, and show clear differences from those of the precursor complex $[\text{Mo}_2(\text{CO})_3(\text{NCMe})_2]$, namely the absence of a resonance at ca. 2.0 ppm assigned to the acetonitrile protons. The observed chemical shifts for complexes **1**, **2** and the free ligands **L**₁ and **L**₂ are summarized in Table 1. The signals from the ligands are shifted to higher fields upon coordination to the metal. This is well noticed in the OH proton, which goes from 8.4 ppm in free **L**₁ to 11.7 ppm in complex **1**, reflecting the loss of electron density. The same can be seen in the NH signal (3.36 in **L**₁ to 9.86 in **1**). Similar trends are observed in complex **2**, suggesting that both ligands coordinate in the neutral form, although the protons assigned to the OH and NH groups cannot be seen in the spectrum of **2**.

The ¹³C NMR spectra of complexes **1** and **2** are also clearly different from those of $[\text{Mo}_2(\text{CO})_3(\text{NCMe})_2]$. The signals of the carbon atoms in the ligands **L**₁ or **L**₂ are shifted in a similar way from their position in the free ligand. No resonances that could be assigned to the carbons of coordinated NCMe of the precursor are detected.



Scheme 1. Synthesis of complexes $[\text{Mo}_2(\text{CO})_3(\text{L}_1)]$ (**1**) and $[\text{Mo}_2(\text{CO})_3(\text{L}_2)]$ (**2**).

Both complexes **1** and **2** exhibited in the FTIR spectra the strong $\nu(\text{C}=\text{O})$ modes, at 2075, 2032, 1997, 1970 and 1951 cm^{-1} (**1**) and 2066, 2001, 1957, 1923, and 1856 cm^{-1} (**2**), shifted from 2089, 2019 and 1942 cm^{-1} in the precursor complex $[\text{Mo}_2(\text{CO})_3(\text{NCMe})_2]$. The larger number of bands indicates the presence of several isomers of these heptacoordinate complexes [16,33], since at most three would be expected in a conic tricarbonyl metal fragment. A band at 1619 cm^{-1} was also observed in **1** (1622 cm^{-1} in **2**), assigned to the $\nu(\text{C}=\text{N})$ of the aromatic ring mode of **L**₁ (**L**₂) ligand. Bands assigned to the $\nu(\text{O}-\text{H})$ and $\nu(\text{N}-\text{H})$ were identified at 3380 and 3268 cm^{-1} in the FTIR spectrum of **1** and at 3368 cm^{-1} in **L**₁. They appeared at 3411 and 3231 cm^{-1} in the spectrum of **2** (3240 and 3326 cm^{-1} in **L**₂).

The presence of these bands supports the proposal that the ligands coordinate in the neutral form in both complexes **1** and **2**.

2.2. Synthesis of materials

The two complexes **1** and **2** were immobilized in two types of materials, MCM-41 and silica. The first one is an ordered and organized material, while silica is an amorphous material.

The MCM-41 (**MCM**) parent material was obtained by a template approach [8], and silica was used as received from a commercial source. After activation, both materials were derivatized by grafting the 3-(chloropropyl)trimethoxysilane spacer, letting it react with the SiOH surface groups, to afford the materials **MCM-Pr-Cl** (Scheme 2) and **Si-Pr-Cl**. According to elemental analysis, the loading of Pr-Cl is found to be 2.0 and 0.43 mmol g^{-1} in **MCM-Pr-Cl** and **Si-Pr-Cl** materials, respectively. Complexes **1** and **2** were then introduced in the presence of triethylamine, so that the resulting anion might react with the pendant chloropropyl chains of the materials, as shown in Scheme 2 for **MCM**. A reported procedure was followed [34]. The new materials obtained, **MCM-Pr-1** and **MCM-Pr-2**, contained approximately 0.59 wt% Mo and 1.16 wt% Mo, corresponding to 0.06 $\text{mmol}_{\text{Mo}} \text{g}^{-1}$ and 0.12 $\text{mmol}_{\text{Mo}} \text{g}^{-1}$, respectively. By the same token, for the silica materials, **Si-Pr-1** and **Si-Pr-2**, loads of 0.52 wt% Mo and 0.029 wt% Mo, corresponding to 0.05 $\text{mmol}_{\text{Mo}} \text{g}^{-1}$ and 0.003 $\text{mmol}_{\text{Mo}} \text{g}^{-1}$, were obtained. These loadings represent a partial functionalization of the parent **Si-Pr-Cl** material reaching 3% and 6% for the **MCM-Pr-1** and **MCM-Pr-2** materials, and 11.6% and 0.7% for the **Si-Pr-1** and **Si-Pr-2** counterparts. These results lead to a low amount of molybdenum in the new materials, showing that such materials can behave as single site catalysts.

Since the coordinated ligands **L**₁ and **L**₂ have two groups, NH and OH, that can be deprotonated in the presence of the base (triethylamine) in the course of the reaction, loss of the OH proton is likely. Reaction between complex **2** and 3-(chloropropyl)trimethoxysilane was carried out separately and the ¹H NMR spectrum of the product indicates this to happen to some extent. The charge obtained in the complex will be balanced by that of the triethylammonium cation. A similar reaction has been reported for the reaction between surface silanol groups and triethylamine [35].

All **MCM** materials were characterized by adequate techniques, but only spectroscopic analyses were performed on the silica materials.

The XRD powder patterns of **MCM-Pr-1** and **MCM-Pr-2** are given in Fig. 1, and are compared to those of the precursors. The pattern of the parent, calcined **MCM** material, shows four reflections in the 2θ range 2–10°, indexed to a hexagonal cell as (100), (110), (200), and (210). The *d* value of the (100) reflection is 38.3 Å, corresponding to a lattice constant of $a = 44.2 \text{ \AA}$ ($=2d_{100}/\sqrt{3}$). The positions of the peaks of **MCM-Pr-Cl**, after functionalizing the walls of the parent host material **MCM** with 3-(chloropropyl)

Table 1
 ^1H and ^{13}C NMR chemical shifts of L_1 , L_2 , $[\text{Mo}_2(\text{CO})_3(\text{L}_1)]$ (**1**), and $[\text{Mo}_2(\text{CO})_3(\text{L}_2)]$ (**2**).

	H ₄	H ₅	H ₆	H ₇	H _{3'}	H _{4'}	H _{5'}	H _{6'}	OH	NH			
L ₁	3.70	3.70	–	–	7.50	6.70	7.30	6.80	8.40	3.36			
1	3.94	3.94	–	–	7.10	7.58	7.04	7.75	11.70	9.86			
L ₂	7.70	7.30	7.30	7.70	8.10	7.00	7.40	7.00	13.10	4.50			
2	7.87	7.60	7.60	7.87	7.25	7.60	7.17	8.07	n.o.	n.o.			
	C ₂	C ₄	C ₅	C ₆	C ₇	C ₈	C ₉	C _{1'}	C _{2'}	C _{3'}	C _{4'}	C _{5'}	C _{6'}
L ₁	n.o.	46.4	46.4	–	–	–	–	110.5	163.3	127.4	115.9	132.7	118.1
1	163.2	44.5	44.5	–	–	–	–	108.6	158.3	120.2	136.6	117.7	130.3
L ₂	151.7	118.0	123.3	122.4	111.5	133.2	140.9	112.6	151.7	117.2	131.7	119.1	126.2
2	157.6	114.5	126.3	126.3	114.5	147.0	147.0	109.7	157.6	117.7	135.5	120.6	129.6

n.o. Not observed.

trimethoxysilane, remain almost unchanged, suggesting the retention of the long range hexagonal symmetry of the host material. A significant reduction of the peaks intensities is observed in the materials **MCM-Pr-1** and **MCM-Pr-2**. This is not interpreted as a loss of crystallinity, but rather as a reduction in the X-ray scattering contrast between the silica walls and pore-filling material, a situation well described in the literature, and also observed for other types of materials [36–38].

Nitrogen adsorption studies at 77 K revealed that the pristine **MCM** sample exhibits a reversible type IV isotherm (Fig. 2), characteristic of mesoporous solids (pore width between 2 and 50 nm, according to the IUPAC [39]). The calculated textural parameters (S_{BET} and V_p) of this material agree with the literature data (Table 2) [40,41]. The capillary condensation/evaporation steps appear in the 0.20–0.40 relative pressures range, and the sharpness of this step reflects the uniform pore size.

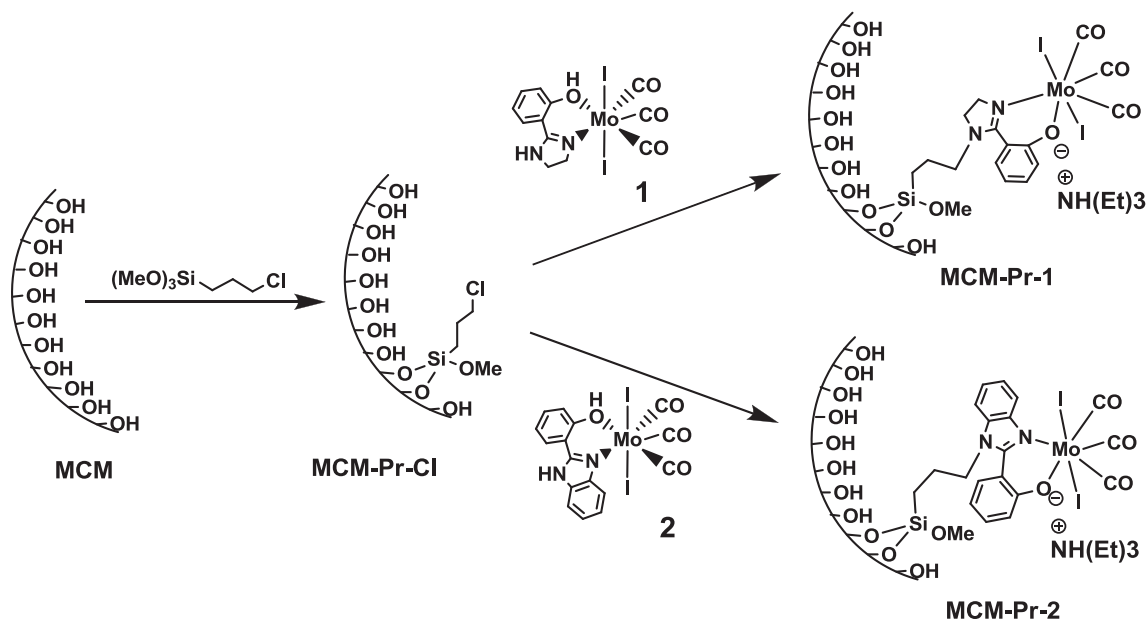
The isotherm of the functionalized material **MCM-Pr-Cl** reveals much lower N_2 uptake, accounting for a decrease in V_p (60%) and a concomitant variation in S_{BET} (43%). These results reflect the immobilization of the ligand on the internal silica surface (Fig. 2, Table 2). Introduction of the complexes **1** and **2** inside the pores induces a further decrease of both S_{BET} and V_p . The decrease in S_{BET} and V_p relative to **MCM** is in agreement with the decrease of the p/p° coordinates of the inflection points of the isotherms after post-synthesis treatments [42].

The height of the capillary condensation steps, which is related to the volume of pore space confined by adsorbate film on the pore walls, is smaller in the case of the modified materials. The maxima of the PSD curves determined by the BJH method, d_{BJH} , decrease concomitantly (Table 2).

Fig. 3 shows the thermogravimetric analyses (TGA) of the materials arising from **MCM** (Scheme 2). Materials **MCM** and **MCM-Pr-Cl** evidence mass losses from 298 K up until ca. 400 K, corresponding to physisorbed water. After that, the organic moieties start to decompose as temperature reaches higher values.

MCM-Pr-Cl loses 15.9% weight, corresponding to 2.3 mmol g^{-1} of **Pr-Cl** ligand inside the **MCM** pores, between 473 and 1073 K. This value closely matches the load of ligand determined from elemental analysis (2.0 mmol g^{-1}).

Both **MCM-Pr-1** and **MCM-Pr-2** lose physisorbed water till 323 K, and organic and organometallic moieties between 323 and 1073 K in two steps. In the first step, 323–518 K, there is a loss of 17.8% weight for **MCM-Pr-1** and 12.8% for **MCM-Pr-2**, associated with release of Mo species. This weight loss, however, exceeds the molybdenum content of each material, known from elemental analysis. On the other hand, the high amount of nitrogen suggests the presence of species different from the immobilized complex, most likely dimethylformamide or triethylamine, used in the synthesis and not totally removed during the calcination (see also ^{13}C NMR spectra). The second step takes place from 523 to 1073 K, with



Scheme 2. Synthesis of materials **MCM-Pr-Cl**, **MCM-Pr-1**, and **MCM-Pr-2**.

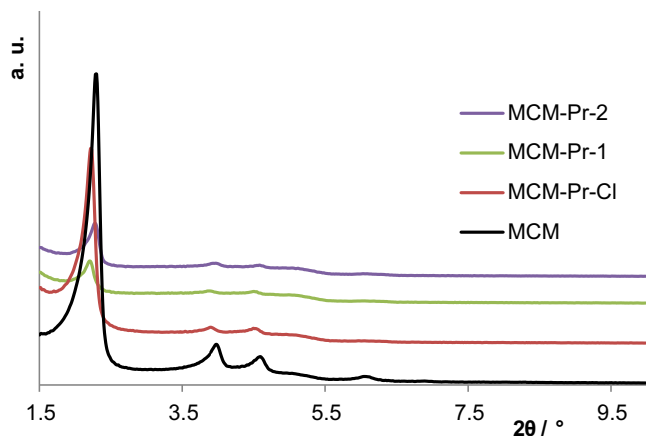


Fig. 1. Powder XRD of materials **MCM**, **MCM-Pr-Cl**, **MCM-Pr-1** and **MCM-Pr-2**.

weight losses of 13.8% for **MCM-Pr-1**, and 8.6% for **MCM-Pr-2**. It is mainly due to the loss of unreacted **Pr-Cl** ligands from the surface of the **MCM** material, in agreement with the thermal profile of the precursor **MCM-Pr-Cl** material.

Similar profiles are obtained for materials **Si-Pr-1** and **Si-Pr-2** (Fig. 3). After the release of physisorbed water till 398 K, weight losses corresponding to 0.03 mmol_{Mo} g⁻¹ and 0.01 mmol_{Mo} g⁻¹, respectively for **Si-Pr-1** and **Si-Pr-2**, reflected the amount of molybdenum obtained from elemental analysis, 0.05 mmol_{Mo} g⁻¹ (**Si-Pr-1**) and 0.003 mmol_{Mo} g⁻¹ (**Si-Pr-2**), respectively. Again a reason for the values found from TGA arises from the content in dimethylformamide and triethylamine, which is confirmed by the high nitrogen amount found from elemental analysis.

The presence of functional groups characteristic of material **MCM-Pr-Cl** and complexes **1** and **2**, after grafting the materials, was checked by FTIR spectroscopy (Fig. 4). In material **MCM-Pr-Cl**, the stretching vibration modes of the mesoporous framework $\nu(\text{Si-O-Si})$ are observed at around 1218, 1066, and 937 cm⁻¹, as in the parent **MCM**. In addition, new bands appear at ca. 2934, 2911 and 2844 cm⁻¹, assigned to the $\nu(\text{C-H})$ stretching of the aliphatic linear chain in **MCM-Pr-Cl**. Signals characteristic of the $\nu(\text{C}\equiv\text{O})$ modes are detected at 2015, 1942, and 1867 cm⁻¹ in material **MCM-Pr-1**, and at 2015 and 1867 cm⁻¹ in **MCM-Pr-2**, respectively. It is also possible to assign bands at 1234, 1053, and 943 cm⁻¹ to the mesoporous framework $\nu(\text{Si-O-Si})$ modes of material **MCM-Pr-1**. The corresponding $\nu(\text{Si-O-Si})$ bands of material **MCM-Pr-2** appear at 1232, 1053, and 945 cm⁻¹.

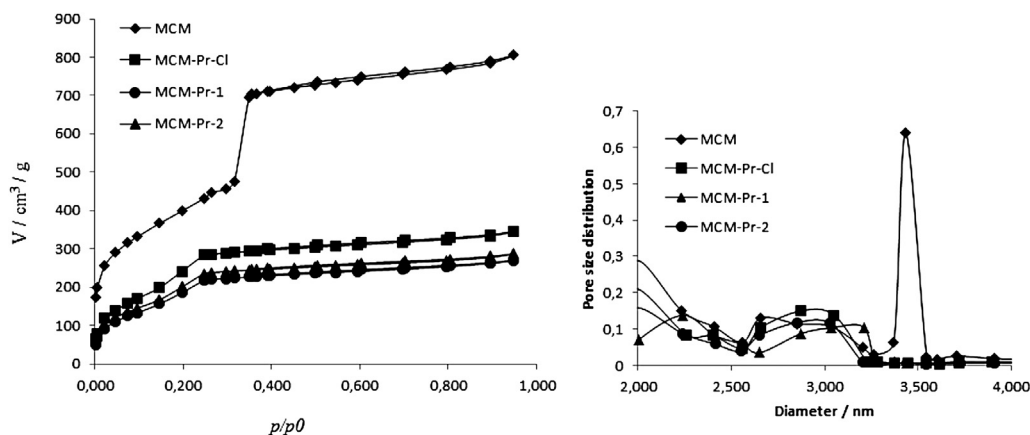


Fig. 2. Nitrogen adsorption and pore size distribution studies of materials **MCM**, **MCM-Pr-Cl**, **MCM-Pr-1** and **MCM-Pr-2**, at 77 K.

Table 2

Textural parameters for host and composite materials from N₂ isotherms at 77 K.

Sample	$d_{100}/\text{\AA}$	$S_{\text{BET}}/\text{m}^2 \text{g}^{-1}$	$\Delta S_{\text{BET}}^{\text{a}}/\%$	$V_{\text{p}}/\text{cm}^3 \text{g}^{-1}$	$\Delta V_{\text{p}}^{\text{b}}/\%$	d_{BJH}/nm
MCM	38.3	1439	—	1.25	—	3.43
MCM-Pr-Cl	39.5	816	-43	0.50	-60	2.90
MCM-Pr-1	38.6	642	-55	0.42	-66	2.87
MCM-Pr-2	38.6	691	-52	0.44	-65	2.85

^a Surface area variation relative to parent MCM.

^b Total pore volume variation relative to parent MCM.

In the FTIR spectra of the silica materials (Fig. 4), $\nu(\text{Si-O-Si})$ bands are observed at 1104 cm⁻¹ in **Si-Pr-Cl**, and at 1105 cm⁻¹ for the two materials **Si-Pr-1** and **Si-Pr-2**. The $\nu(\text{C}\equiv\text{O})$ modes can be seen at 2000 and 1874 cm⁻¹ (**Si-Pr-1**) and 2041 and 1888 cm⁻¹ (**Si-Pr-2**). The small amount of metal complex grafted in the materials makes these bands relatively weak, leading to some uncertainty in the wavelengths. The $\nu(\text{C-H})$ stretching modes of the aliphatic linear chain are observed in all silica materials in the range 2952–2815 cm⁻¹, confirming the presence of the spacer.

The materials were also characterized by ¹³C CP MAS-DD and ²⁹Si CP MAS-DD solid state NMR.

The ¹³C CP MAS-DD spectrum (not shown) of **MCM-Pr-Cl** presents resonances of the propyl chain at 9.8 (Si-CH₂), 26.1 (CH₂-CH₂-CH₂) and 45.8 (Cl-CH₂) ppm. The **MCM-Pr-1** material shows three resonances of the propyl chain protons at 10.5 (Si-CH₂), 26.6 (CH₂-CH₂-CH₂) and 47.6 (Cl-CH₂) ppm, while for material **MCM-Pr-2** the carbon resonances are observed at 10.4, 26.5, and 47.5 ppm. Both are shifted relative to the signals of **MCM-Pr-Cl**. For materials with the Mo core, it is difficult to observe the signals of the aromatic carbons from the **L**₁ and **L**₂ ligands. In both spectra, signals at 31.4, 36.8 and 164.0 ppm arise from the solvent used, dimethylformamide. This solvent reacts with the materials surface silanol groups and is very difficult to eliminate completely.

The ²⁹Si CP MAS-DD NMR spectrum of pristine **MCM**, Fig. 5, displays three resonances at -112.0, -101.7 and -91.8 ppm, characteristic of Q⁴, Q³ and Q² species of the silica framework, respectively. In **MCM-Pr-Cl**, the Q⁴, Q³ and Q² signals shift to -110.9, -100.6 and -92.5 ppm, while three broad signals at -66.7, -57.4 and -48.5 ppm, assigned to T³, T² and T¹ organosilica species, appear in the spectrum. Reaction with the organometallic complexes [Mo₂(CO)₃(**L**₁/**L**₂)], to obtain **MCM-Pr-1** and **MCM-Pr-2**, does not significantly change the ²⁹Si CP MAS-DD NMR spectra. In **MCM-Pr-1** Q⁴, Q³ and Q² signals are observed at -110.2, -101.2 and -91.8 ppm, and two signals at -66.2, -58.0 ppm are assigned to T³ and T² organosilica species,

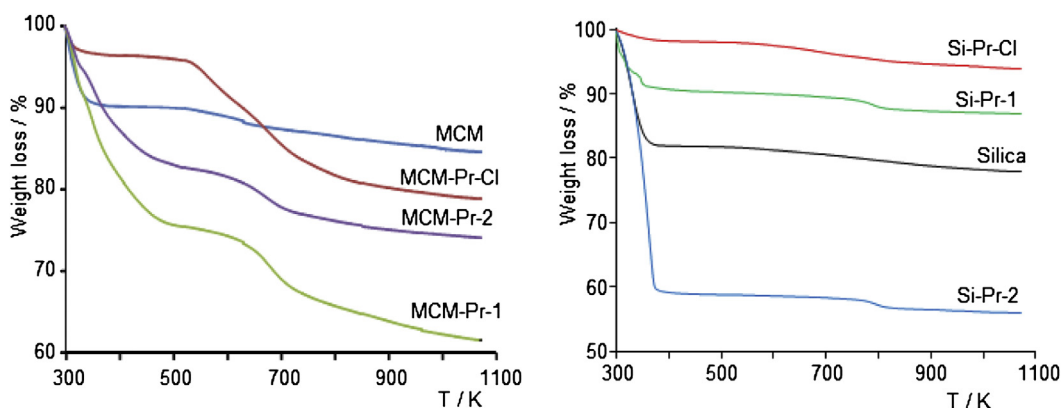


Fig. 3. Thermogravimetric profiles of materials **MCM**, **MCM-Pr-Cl**, **MCM-Pr-1**, and **MCM-Pr-2** (left) and **Silica**, **Si-Pr-Cl**, **Si-Pr-1**, and **Si-Pr-2** (right).

slightly shifted. In material **MCM-Pr-2**, the same trend was observed, with the Q^4 , Q^3 and Q^2 signals at -109.9 , -101.1 and -91.0 ppm, and the two broad signals at -66.5 , -58.0 ppm, assigned to T^3 and T^2 organosilica species.

2.3. Catalytic studies

Both complexes, $[Mo_2(CO)_3(L_1)]$ (**1**) and $[Mo_2(CO)_3(L_2)]$ (**2**), and the final materials **MCM-Pr-1**, **MCM-Pr-2**, **Si-Pr-1**, **Si-Pr-2**, were

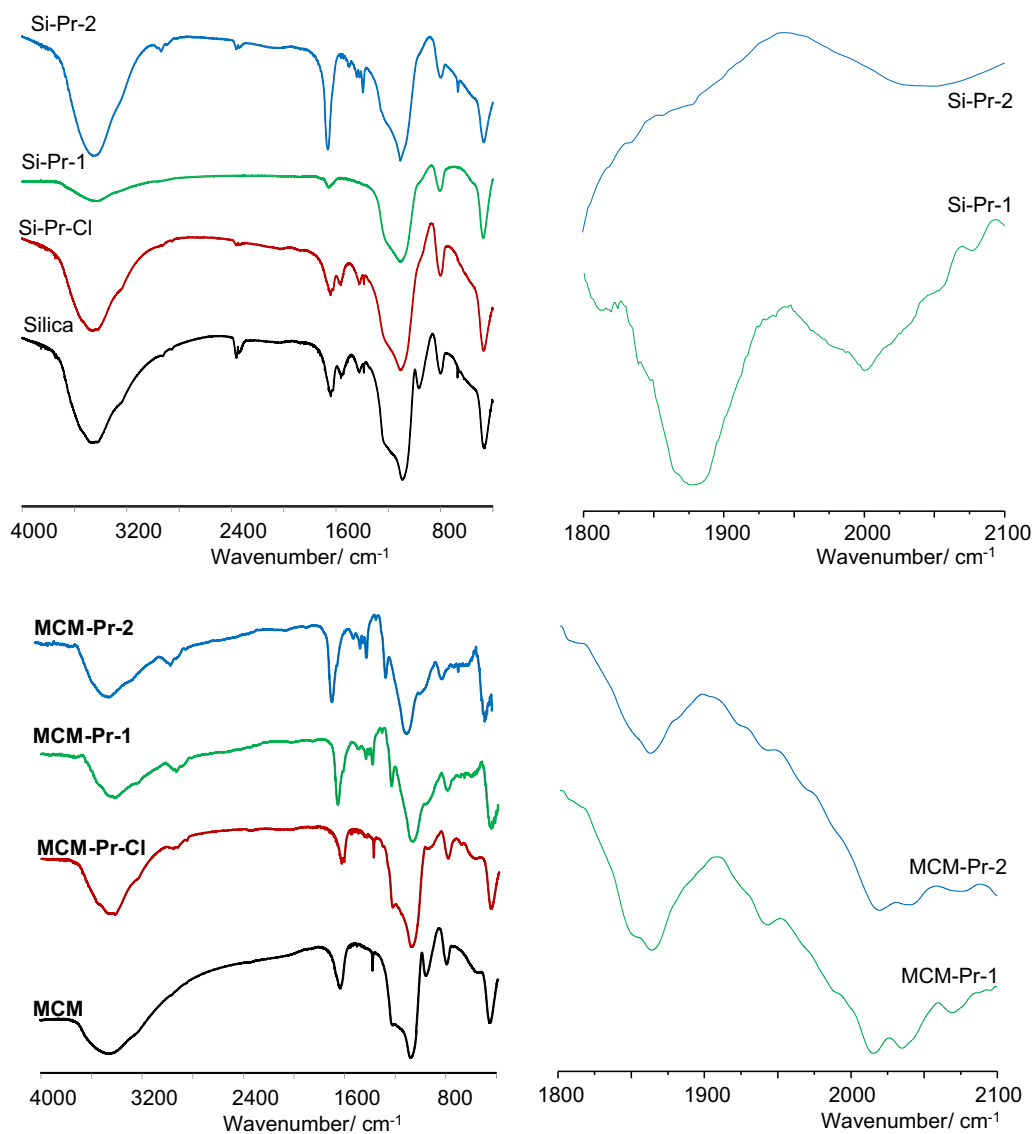


Fig. 4. Infrared spectra of materials **MCM**, **MCM-Pr-Cl**, **MCM-Pr-1**, and **MCM-Pr-2** (bottom) and **Silica**, **Si-Pr-Cl**, **Si-Pr-1**, and **Si-Pr-2** (top) with expansion of the 1800–2100 cm^{-1} range.

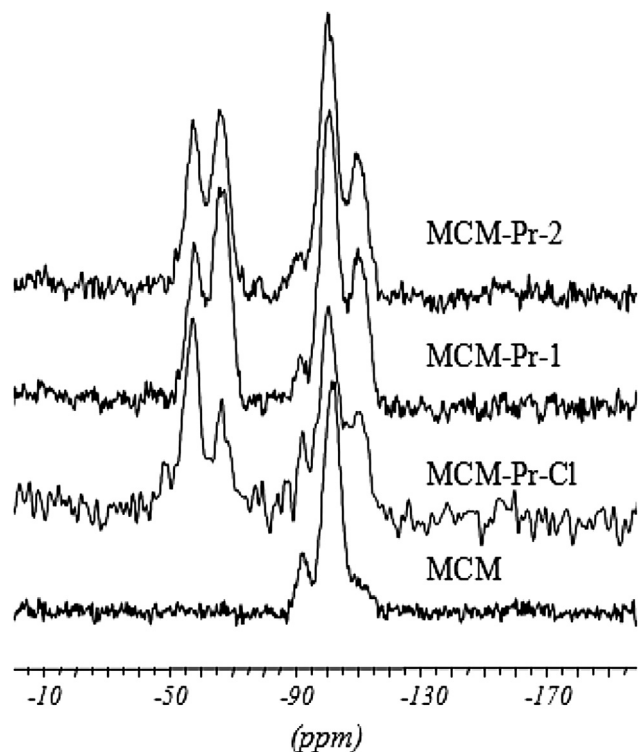


Fig. 5. ^{29}Si CP MAS-DD spectra of MCM, MCM-Pr-Cl, MCM-Pr-1 and MCM-Pr-2.

tested as catalyst precursors for olefin epoxidation using two types of substrates. The first one comprises simple olefins, such as *cis*-cyclooctene (cy8), 1-octene (1-oct), and styrene (sty), while the second one includes multifunctional olefins: geraniol (ger), *trans*-hex-2-en-1-ol (*trans*), *cis*-hex-3-en-1-ol (*cis*), and *R*(+)-limonene (*R*-lim). All reactions were carried out using *tert*-butylhydroperoxide (TBHP in decane) as oxygen donor, in dichloromethane, at 328 K (see details in Experimental section). No reaction took place in the absence of a catalyst.

All tested catalysts are 100% selective towards the epoxide in the oxidation of *cis*-cyclooctene (cy8). Catalysts **1** and **2** show much higher conversions than all the heterogeneous catalysts. Among these, only **Si-Pr-1** presents a fair conversion of substrate. The silica based catalysts lead to slightly higher conversions than those supported on MCM.

Reaction kinetics also shows that the homogeneous catalysts achieve higher rates than the corresponding heterogeneous counterparts, as evidenced in Fig. 6. Catalyst **2** and MCM-Pr-2 reach maximum product yield after ca. 6 h reaction time, though the initial rate is much higher for **2**. There seems to be an induction period for catalyst **Si-Pr-2**, since the product is barely detected before 8 h. Such differences between the two heterogeneous catalysts may arise mostly from structural/morphological differences of the inorganic hosts.

The oxidation of 1-octene, an unbranched (not activated) terminal olefin, is achieved with medium conversions by the MCM materials (entries 9 and 10), while there is no conversion when the catalyst is supported on silica (Table 3, entries 11–12), and the two complexes present very low conversions. The highest selectivity towards the epoxide was observed with the most active materials MCM-Pr-1 and MCM-Pr-2 as catalyst (entries 9–10).

Styrene is converted very inefficiently into the epoxide by all the catalysts and the selectivity is also rather low, except with the material MCM-Pr-2, when it reaches 73%. A more detailed analysis of the catalytic reaction reveals that the styrene epoxide formed

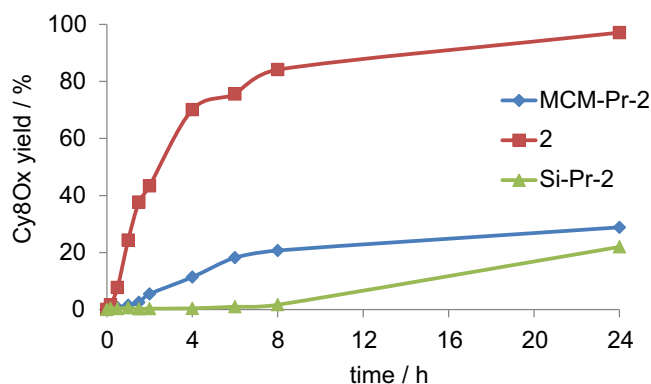


Fig. 6. Kinetic profiles of *cis*-cyclooctene epoxidation mediated by **2**, MCM-Pr-2 and Si-Pr-2 catalysts.

continues to react, yielding benzaldehyde, which results from oxidative cleavage of the epoxide [43].

All catalysts convert *trans*-hex-2-en-1-ol into its epoxide, but catalysts **1**, **2** and **Si-Pr-1** present higher conversion and selectivity to the epoxide (Table 3, entries 19, 20 and 23). In particular **Si-Pr-1** exhibits 98% conversion with 99% selectivity to the epoxide. The other catalysts, namely the two MCM based materials, MCM-Pr-1 and MCM-Pr-2, behave very poorly.

The oxidation of *cis*-hex-3-en-1-ol is very selective (100%) displaying medium conversions (entries 25, 26, 29) with catalysts **1** (28%), **2** (59%) and **Si-Pr-1** (43%). These are the same catalysts active in the oxidation of *trans*-hex-2-en-1-ol. MCM-Pr-2 exhibits a residual activity (conversion 4%), while the others do not catalyze the reaction (entries 27 and 30).

The two remaining substrates, *R*(+)-limonene and geraniol, have two C=C bonds, so two different epoxides are possible. Those favored by the catalysts being studied are sketched in Table 3 (epoxidation in the ring, for *R*(+)-limonene, and in the 2,3 positions, for geraniol).

In the oxidation of *R*(+)-limonene, the three catalysts **1**, **2** and **Si-Pr-1** lead to higher conversions, though **2** is the less active. However, the high conversions achieved by **1** and **Si-Pr-1** (80% and 86%, Table 3, entries 31 and 35) coexist with the lowest selectivities towards the endocyclic epoxide (37% and 41%), the product formed in larger amounts being the diepoxide product (in both endo- and exo-cyclic positions). The other three catalysts associate a much smaller activity (conversions from 6 to 15%) with higher selectivities (from 73 to 77%), though still far from 100%.

In the oxidation of geraniol, MCM-Pr-1 and Si-Pr-2 continue to be the least active catalysts, with low conversions of 27 and 19%, respectively, and very low selectivity for the 2,3-epoxide. The other catalysts lead to higher conversions, namely **1**, **2** and **Si-Pr-1**, which were also more active towards the other substrates. They also display the highest selectivity, favoring the formation of the 2,3-epoxide (Table 3, entries 37, 38, 41). The second product formed is the diepoxide, and a mixture of the two products is always obtained independent of the chosen catalyst (homogeneous or heterogeneous, MCM or silica based).

In general, complete selectivity was only observed across all catalysts for *cis*-cyclooctene and *cis*-hex-3-en-1-ol, but conversions were higher when oxidizing *cis*-cyclooctene. Oxidation of styrene was found to yield benzaldehyde globally as major product, which arises from oxidative cleavage of the epoxide. After 24 h reaction time, benzaldehyde is the major product independently of the catalytic systems, except when using material MCM-Pr-2 as catalyst precursor.

Epoxidation of *R*(+)-limonene and geraniol was found to occur with fair to good substrate conversion, and epoxide products were

Table 3Olefin oxidation catalyzed by complexes $\text{Mo}_2(\text{CO})_3(\text{L}_1)$ (**1**), $\text{Mo}_2(\text{CO})_3(\text{L}_2)$ (**2**), and materials **MCM-Pr-1**, **MCM-Pr-2**, **Si-Pr-1**, and **Si-Pr-2**.

Entry	Epoxide ^a	Catalyst	Conversion ^{b,c} [%]	Selectivity ^c [%]
1		1	93	100
2		2	97	100
3		MCM-Pr-1	2	100
4		MCM-Pr-2	29	100
5		Si-Pr-1	42	100
6		Si-Pr-2	22	100
7		1	19	78 ^d
8		2	10	83 ^d
9		MCM-Pr-1	51	98 ^d
10		MCM-Pr-2	45	100
11		Si-Pr-1	0	0
12		Si-Pr-2	0	0
13		1	32	42 ^e
14		2	6	6 ^e
15		MCM-Pr-1	22	22 ^e
16		MCM-Pr-2	17	73 ^e
17		Si-Pr-1	40	14 ^e
18		Si-Pr-2	6	25 ^e
19		1	61	87 ^f
20		2	69	84 ^f
21		MCM-Pr-1	6	39 ^f
22		MCM-Pr-2	8	50 ^f
23		Si-Pr-1	98	99 ^f
24		Si-Pr-2	5	33 ^f
25		1	28	100
26		2	59	100
27		MCM-Pr-1	0	0
28		MCM-Pr-2	4	100
29		Si-Pr-1	43	100
30		Si-Pr-2	0	0
31		1	80/31/32 ^{g,h}	37/67/52 ^{g,h}
32		2	31	75 ^h
33		MCM-Pr-1	8	73 ^h
34		MCM-Pr-2	15	77 ^h
35		Si-Pr-1	86/99/52 ^{g,h}	41/27/26 ^{g,h}
36		Si-Pr-2	6	77 ^h
37		1	82	66 ⁱ
38		2	96	68 ⁱ
39		MCM-Pr-1	27	17 ⁱ
40		MCM-Pr-2	63	66 ⁱ
41		Si-Pr-1	72	83 ⁱ
42		Si-Pr-2	19	14 ⁱ

^a All reactions carried out in CH_2Cl_2 in the presence of 200 mol% oxidant (TBHP) and 1 mol% of molybdenum catalyst at 328 K.^b Calculated after 24 h.^c Calculated as "Yield of epoxide"/"Conversion" \times 100% after 24 h.^d Octanal formed as by-product.^e Benzaldehyde formed as by-product.^f α -Hydroxyketone formed as by-product.^g Values correspond to 1st, 2nd and 3rd recycle runs, respectively.^h Diepoxide formed as by-product.ⁱ 6,7-Epoxide formed as by-product.

obtained as mixtures of isomers. Still the major products were the diepoxide (in *R*(+)-limonene) and the allylic position epoxide (geraniol).

Catalyst robustness, namely its resistance to leaching and recycling, was also evaluated. Such experiments were carried out for the more active systems, complex **1** and material **Si-Pr-1**, in the epoxidation of *R*(+)-limonene. The results from recycling experiments (Table 3, entries 31 and 35) show that catalyst **1** suffers severe deactivation just after the first cycle, while the heterogeneous catalyst **Si-Pr-1** is only deactivated at the third cycle, evidencing one advantage of immobilizing the homogeneous catalysts. The selectivity exhibited by this catalyst drops to 26%.

Leaching experiments were carried out in the epoxidation of *R*(+)-limonene with catalyst **Si-Pr-1**. The heterogeneous catalyst was filtered after 2 h reaction time (at which substrate conversion was 10%), and the reaction in the solution was monitored up to 24 h. The conversion did not change, meaning that the catalyst is really heterogeneous in nature showing virtually no leaching to the liquid phase.

3. Conclusions

Two new complexes [$\text{Mo}_2(\text{CO})_3(\text{L}_1)$] (**1**) or [$\text{Mo}_2(\text{CO})_3(\text{L}_2)$] (**2**) with the ligands $\text{L}_1 = 2$ -(2'-hydroxyphenyl)imidazoline and $\text{L}_2 = 2$ -(2'-hydroxyphenyl)benzimidazole were synthesized and immobilized in MCM-41 and silica by grafting using with a (3-chloropropyl)trimethylsilane spacer.

Spectroscopic data and elemental analysis indicated that the ligands coordinated in an unusual neutral form. The catalytic activity of the two complexes and the four materials in the oxidation of several substrates, in the presence of TBHP, under homogeneous and heterogeneous conditions, respectively, was studied. Only complex **2** could epoxidize *cis*-cyclooctene selectively with 97% conversion, and complex **1** immobilized in silica converted 98% of *trans*-hex-2-en-1-ol to the epoxide selectively. In some systems, no reaction took place. Although there are not clear trends, complex **1** in silica (**Si-Pr-1**) was the best combination, generally improving the performance of complex **1** in homogeneous catalysis, with the total failure to oxidize 1-octene. The best performance of the homogeneous catalysts may be associated with deprotonation of the ligand during the immobilization procedure.

4. Experimental

4.1. General procedures

All reagents were obtained from Aldrich and used as received. Commercial grade solvents were dried and deoxygenated by standard procedures (diethyl ether and toluene over sodium/benzophenone ketyl; methanol, dichloromethane and dimethylformamide over calcium hydride), distilled under nitrogen, and kept over 4 Å molecular sieves, except methanol (over 3 Å molecular sieves). The ligands 2-(2'-hydroxyphenyl)imidazoline (L_1), 2-(2'-hydroxyphenyl)benzimidazole (L_2) [29–31], and the precursor complex [$\text{Mo}_2(\text{CO})_3(\text{NCMe})_2$] [16] was prepared according to literature methods.

MCM-41 and functionalized materials were prepared by adopting a methodology previously described, using [$(\text{C}_{14}\text{H}_{33})\text{N}(\text{CH}_3)_3\text{Br}$] as template agent [8]. Prior to the grafting experiment, physisorbed water was removed from MCM by heating at 453 K in vacuum (10^{-2} Pa) for 2 h.

FTIR spectra were obtained as KBr pellets (complexes) and Diffuse Reflectance (DRIFT) measurements (materials) on a Nicolet 6700 in the 400–4000 cm^{-1} range using 1 cm^{-1} resolution. Microanalyses for C, H, N, and Mo quantification were performed at

CACTI, University of Vigo (C, H, and N analyses on a Fisons EA 1108, and Mo on a Perkin Elmer Optima 4300DV using In as internal standard).

^1H and ^{13}C solution NMR spectra were obtained with a Bruker Avance 400 spectrometer. Solid state ^{29}Si and ^{13}C NMR measurements were performed at room temperature on a Bruker MSL 300P spectrometer operating at 59.60 and 75.47 MHz for the observation of ^{29}Si and ^{13}C resonances, respectively. The standard magic angle spinning (MAS) cross polarization – dipolar decoupling RF pulse sequence (CP-DD) was used under about 4 kHz spinning rate. For the acquisition of ^{29}Si spectra, 5 ms contact time was chosen, 6 s recycling delay, and a number of scans always higher than 3000 were selected; the Hartmann-Hahn condition [44] was optimized using tetrakis(trimethylsilyl)silane, and tetramethylsilane (TMS) was the external reference to set the chemical shift scale. ^{13}C spectra were recorded with 2 ms contact time, 4 s recycling delay and a number of scans higher than 900. The Hartmann–Hahn condition was optimized using glycine, also the external reference to set the chemical shift scale (^{13}CO at 176.1 ppm).

Powder XRD measurements were taken on a Philips Analytical PW 3050/60 X'Pert PRO (theta/2 theta) equipped with X'Celerator detector and with automatic data acquisition (X'Pert Data Collector (v2.0b) software), using monochromatized Cu-K α radiation as incident beam, 40 kV–30 mA.

TGA studies were performed using a Perkin–Elmer TGA7 thermobalance system at a heating rate of 10 $^\circ\text{C min}^{-1}$ under N_2 .

The N_2 adsorption/desorption measurements were obtained in an automatic apparatus (ASAP 2010; Micromeritics). BET specific surface areas (S_{BET} , p/p° from 0.03 to 0.13) and specific total pore volume, V_p were estimated from N_2 adsorption isotherms measured at 77 K. The pore size distributions (PSD) were calculated by the BJH method using the modified Kelvin equation with correction for the statistical film thickness on the pore walls [45,46]. The statistical film thickness was calculated using Harkins–Jura equation [47,48] in the p/p° range from 0.1 to 0.95. Prior to the measurements, samples were degassed, and physisorbed water was removed by heating at 723 K for MCM and 413 K for the derivatized materials (to minimize the destruction of the functionalities) in vacuum for 2 h.

4.2. Syntheses

4.2.1. [$\text{Mo}_2(\text{CO})_3(\text{L}_1)$] **1**

A solution of 2-(2'-hydroxyphenyl)imidazoline (0.5 mmol, 0.0811 g) in methanol was added to a stirred solution of [$\text{Mo}_2(\text{CO})_3(\text{MeCN})_2$] (0.5 mmol, 0.2575 g) also in methanol. The mixture was stirred overnight, under inert atmosphere. The brown solid formed was filtered, washed with diethyl ether and dried under vacuum.

Yield: 0.224 g, 75% yield. Anal. Calc. for $\text{Mo}_2\text{N}_2\text{O}_4\text{C}_{12}\text{H}_{10}$: C 24.18, H 1.69, N 4.70. Found: C 24.57, H 2.05, N 4.87.

IR (KBr, ν/cm^{-1}): 3380 (w), 3268 (w), 2929 (w), 2858 (w), 2075 (s), 2032 (s), 1997 (s), 1970 (s), 1951 (s), 1619 (s), 1587 (s), 1560 (s), 1498 (m), 1452 (m), 1373 (m), 1346 (m), 1309 (m), 1288 (m), 1251 (m), 1199 (w), 1164 (w), 1143 (w), 1097 (w), 1033 (m), 981 (m), 823 (w), 771 (w), 742 (m), 590 (m), 528 (m), 476 (m).

^1H NMR (400.10 MHz, DMSO, r.t., δ ppm): 3.94 (s, 4H, H_4/H_5), 7.04 (t, 1H, H_5'), 7.10 (d, 1H, H_3'), 7.58 (t, 1H, H_4'), 7.75 (d, 1H, H_6'), 9.86 (s, 1H, NH), 11.7 (s, 1H, OH).

^{13}C NMR (100.25 MHz, DMSO, r.t., δ ppm): 44.5 (C_4/C_5), 108.6 (C_1'), 117.7 (C_5'), 120.2 (C_3'), 130.3 (C_6'), 136.6 (C_4'), 158.3 (C_2'), 163.2 (C_2).

4.2.2. [$\text{Mo}_2(\text{CO})_3(\text{L}_2)$] **2**

A solution of 2-(2'-hydroxyphenyl)benzimidazole (0.5 mmol, 0.1051 g) in methanol was added to a stirred solution of

[Mol₂(CO)₃(MeCN)₂] (0.5 mmol, 0.2575 g) also in methanol. The mixture was stirred overnight, under inert atmosphere. The brown solid formed was filtered, washed with diethyl ether and dried under vacuum.

Yield: 0.252 g, yield 83%. Anal. Calc. for Mol₂N₂O₄C₁₆H₁₀: C 29.84, H 1.57, N 4.35. Found: C 29.48, H 2.03, N 4.67.

IR (KBr, ν/cm^{-1}): 3411 (vs), 3231 (w), 3088 (w), 3038 (w), 2952 (w), 2908 (w), 2846 (w), 2735 (w), 2066 (s), 2001 (s), 1957 (s), 1923 (s), 1856 (m), 1622 (s), 1558 (m), 1462 (m), 1458 (m), 1239 (m), 1102 (m), 1082 (m), 744 (m).

¹H NMR (400.10 MHz, DMSO, r.t., δ ppm): 7.17 (t, 1H, H_{5'}), 7.25 (d, 1H, H_{3'}), 7.60 (m, 3H, H₄/H₅/H₆), 7.87 (m, 2H, H₄/H₇), 8.07 (H_{6'}).

¹³C NMR (100.25 MHz, DMSO, r.t., δ ppm): 109.7 (C_{1'}), 114.5 (C₄/C₇), 117.7 (C_{3'}), 120.6 (C_{5'}), 126.3 (C₅/C₆), 129.6 (C_{6'}), 135.5 (C_{4'}), 147.0 (C₈/C₉), 157.6 (C₂/C_{2'}).

4.2.3. MCM-Pr-Cl

2.0 mL of 3-(chloropropyl)trimethoxysilane was added to a suspension of 1 g of MCM-41 in 30 mL of toluene, and allowed to reflux for 24 h. The yellow suspension was filtered, washed with 4 × 20 mL dichloromethane, and dried under vacuum.

Anal. Found: C 7.21, H 1.73.

IR (KBr, ν/cm^{-1}): 3404 (vs), 2934 (w), 2911 (w), 2844 (w), 1621 (m), 1615 (m), 1384 (m), 1218 (s), 1066 (vs), 937 (w), 789 (m), 668 (w), 568 (w), 448 (s).

¹³C CP/MAS (DD) NMR (δ ppm): 9.8 (Si-CH₂), 26.1 (-CH₂-), 45.8, 46.9 (Cl-CH₂).

²⁹Si CP/MAS (DD) NMR (δ ppm): -48.5 (T¹), -57.4 (T²), -66.7 (T³), -92.5 (Q²), -100.6 (Q³), -110.9 (Q⁴).

4.2.4. MCM-Pr-1 and MCM-Pr-2

The complex **1** or **2** (3 mmol) was dissolved in dimethylformamide, and then triethylamine (3.8 mmol) was added. 1 g of **MCM-Pr-Cl** was added to this solution, at 273 K, and then left at room temperature for 12 h. The suspension was filtered, washed with 2 × 20 mL dichloromethane, and dried under vacuum.

4.2.4.1. **MCM-Pr-1**. Anal. Found: C 14.42, H 3.12, N 3.09, Mo 0.59.

IR (KBr, ν/cm^{-1}): 3390 (vs), 3224 (w), 2939 (w), 2922 (w), 2870 (w), 2792 (w), 2008 (w), 1923 (w), 1842 (w), 1655 (s), 1483 (w), 1385 (w), 1234 (m), 1053 (vs), 943 (s), 781 (m), 442 (s).

¹³C CP/MAS (DD) NMR (δ ppm): 10.5 (Si-CH₂), 26.6 (-CH₂-), 47.6 (Cl-CH₂).

²⁹Si CP/MAS (DD) NMR (δ ppm): -58.0 (T²), -66.2 (T³), -91.8 (Q²), -101.2 (Q³), -110.2 (Q⁴).

4.2.4.2. **MCM-Pr-2**. Anal. Found: C 16.42, H 3.52, N 3.85, Mo 1.16.

IR (KBr, ν/cm^{-1}): 3390 (vs), 3219 (w), 2931 (w), 2920 (w), 2868 (w), 2792 (w), 2008 (w), 1842 (w), 1655 (vs), 1483 (w), 1437 (w), 1385 (m), 1232 (m), 1053 (vs), 945 (m), 781 (m), 447 (s).

¹³C CP/MAS (DD) NMR (δ ppm): 10.4 (Si-CH₂), 26.5 (-CH₂-), 47.5 (Cl-CH₂).

²⁹Si CP/MAS (DD) NMR (δ ppm): -58.0 (T²), -66.5 (T³), -91.0 (Q²), -101.1 (Q³), -109.9 (Q⁴).

4.2.5. Silica-Pr-Cl

2.0 mL of 3-(chloropropyl)trimethoxysilane was added to a suspension of 1 g of silica in 30 mL of toluene, and allowed to reflux for 24 h. The yellow suspension was filtered, washed with 4 × 20 mL dichloromethane, and dried under vacuum.

Anal. Found: C 1.56, H 0.51.

IR (KBr, ν/cm^{-1}): 3373 (s), 2886 (w), 1622 (w), 1205 (vs), 1080 (vs), 946 (m), 789 (m), 462 (s).

¹³C CP/MAS (DD) NMR (δ ppm): 9.6 (Si-CH₂), 26.1 (-CH₂-), 45.8 (Cl-CH₂).

²⁹Si CP/MAS (DD) NMR (δ ppm): -52.4 (T¹), -60.6 (T²), -70.4 (T³), -96.6 (Q²), -103.1 (Q³), -114.6 (Q⁴).

4.2.6. Silica-Pr-1 and silica-Pr-2

The complex **1** or **2** (3 mmol) was dissolved in dimethylformamide, and then triethylamine (3.8 mmol) was added. 1 g of **silica-Pr-Cl** was added to this solution, at 273 K, and then left at room temperature for 12 h. The suspension was filtered, washed with 2 × 20 mL dichloromethane, and dried under vacuum.

4.2.6.1. **Silica-Pr-1**. Anal. Found: C 2.79, H 0.64, N 0.41, Mo 0.52.

IR (KBr, ν/cm^{-1}): 3425 (s), 2952 (w), 2917 (w), 2871 (w), 1998 (w), 1867 (w), 1652 (m), 1105 (vs), 802 (m), 473 (s).

¹³C CP/MAS (DD) NMR (δ ppm): 9.0 (Si-CH₂), 25.8 (-CH₂-), 64.6 (Cl-CH₂), 115–160 broad band aromatic carbons.

²⁹Si CP/MAS (DD) NMR (δ ppm): -60.6 (T²), -65.5 (T³), -93.3 (Q²), -104.8 (Q³), -112.96 (Q⁴).

4.2.6.2. **Silica-Pr-2**. Anal. Found: C 5.11, H 1.04, N 1.62, Mo 0.029.

IR (KBr, ν/cm^{-1}): 3400 (vs), 2924 (w), 2910 (w), 2839 (w), 2744 (w), 2007 (w), 1838 (w), 1653 (vs), 1456 (w), 1402 (w), 1308 (m), 1224 (s), 1090 (vs), 779 (m), 613 (w), 453 (m).

¹³C CP/MAS (DD) NMR (δ ppm): 9.8 (Si-CH₂), 25.4 (-CH₂-), 65.9 (Cl-CH₂).

²⁹Si CP/MAS (DD) NMR (δ ppm): -60.6 (T²), -72.0 (T³), -94.95 (Q²), -106.4 (Q³), -116.2 (Q⁴).

4.3. Catalytic tests

The complexes and materials were tested in the catalytic epoxidation of *cis*-cyclooctene (cy8), 1-octene (1-oct), styrene (sty), geraniol (ger), *cis*-hex-3-en-1-ol (*cis*), *trans*-hex-2-en-1-ol (*trans*) and *R*(+)-limonene (*R*-lim), using *tert*-butylhydroperoxide (TBHP) as oxidant. The catalytic oxidation tests were carried out at 328 K under normal atmosphere in a reaction vessel equipped with a magnetic stirrer and a condenser. In a typical experiment the vessel was loaded with olefin or alcohol (100 mol%), internal standard (dibutyl ether), catalysts (1 mol%), oxidant (200 mol%), and 3 mL of solvent. Addition of the oxidant determines the initial time of the reaction. The course of the reactions was monitored by quantitative GC-analysis by collecting samples at 10, 30 min, 1 h and 1.5 h, then at 2, 4, 6, 8, and 24 h of reaction. These samples were treated as described previously prior to injection in the GC column [43].

4.3.1. *Epoxidation of cis-cyclooctene (cy8), 1-octene (1-oct), styrene (sty), R(+)-limonene(R(+)-lim), geraniol (ger), cis-3-hexen-1-ol (cis), and trans-2-hexen-1-ol (trans)*

Substrate (800 mg): 7.3 mmol of *cis*-cyclooctene, 7.7 mmol of styrene, 5.2 mmol of geraniol, 7.1 mmol of 1-octene, 5.87 mmol of *R*(+)-limonene, 7.99 mmol of *cis*-hex-3-en-1-ol, and 7.99 mmol of *trans*-hex-2-en-1-ol, 800 mg dibutyl ether (internal standard), 1 mol% of catalyst, 2.65 mL of TBHP (5.5 M in *n*-decane) and 3 mL of dichloromethane (CH₂Cl₂).

Acknowledgements

The authors thank FCT, POCl and FEDER (projects PTDC/QUI/71576/2006, PEst-OE/QUI/UI0612/2013, PEst-OE/QUI/UI0100/2013) for financial support. MSS and CIF thank FCT for research grants (SFRH/BD/48640/2008 and SFRH/BD/81029/2011).

References

- [1] M.H. Valkenberg, W.F. Hölderich, Catal. Rev. 44 (2002) 321–374.
- [2] A. Taguchi, F. Schüth, Micropor. Mesopor. Mater. 77 (2005) 1–45.

- [3] C.T. Kresge, M.E. Leonowicz, W.J. Roth, J.C. Vartuli, J.S. Beck, *Nature* 359 (1992) 710–712.
- [4] J.S. Beck, J.C. Vartuli, W.J. Roth, M.E. Leonowicz, C.T. Kresge, K.D. Schmitt, C.T.W. Chu, D.H. Olson, E.W. Sheppard, S.B. McCullen, J.B. Higgins, J.L. Schlenker, *J. Am. Chem. Soc.* 114 (1992) 10834–10843.
- [5] C.D. Nunes, M. Pillinger, A.A. Valente, I.S. Gonçalves, J. Rocha, P. Ferreira, F.E. Kühn, *Eur. J. Inorg. Chem.* (2002) 1100–1107.
- [6] T.A. Fernandes, C.D. Nunes, P.D. Vaz, M.J. Calhorda, P. Brandão, J. Rocha, I.S. Gonçalves, A.A. Valente, L.P. Ferreira, M. Godinho, P. Ferreira, *Micropor. Mesopor. Mater.* 112 (2008) 14–25.
- [7] J. Gimenez, C.D. Nunes, P.D. Vaz, A.A. Valente, P. Ferreira, M.J. Calhorda, *J. Mol. Catal. A* 256 (2006) 90–98.
- [8] C.D. Nunes, A.A. Valente, M. Pillinger, A.C. Fernandes, C.C. Romão, J. Rocha, I.S. Gonçalves, *J. Mater. Chem.* 12 (2002) 1735–1742.
- [9] M. Vasconcellos-Dias, C.D. Nunes, P.D. Vaz, P. Ferreira, P. Brandão, V. Félix, M.J. Calhorda, *J. Catal.* 256 (2008) 301–311.
- [10] D.M. Ford, E.E. Simanek, D.F. Shantz, *Nanotechnology* 16 (2005) S458–S475.
- [11] M. Pillinger, C.D. Nunes, P.D. Vaz, A.A. Valente, I.S. Gonçalves, P.J.A. Ribeiro-Claro, J. Rocha, L.D. Carlos, F.E. Kühn, *Phys. Chem. Chem. Phys.* 4 (2002) 3098–3105.
- [12] P. Oliveira, A. Machado, A.M. Ramos, I. Fonseca, F.M. Braz Fernandes, A.M. Botelho do Rego, J. Vital, *Micropor. Mesopor. Mater.* 120 (2009) 432–440.
- [13] M.S. Saraiva, S. Quintal, F.C.M. Portugal, T.A. Lopes, V. Félix, J.M.F. Nogueira, M. Meireles, M.G.B. Drew, M.J. Calhorda, *J. Organomet. Chem.* 693 (2008) 3411–3418.
- [14] M.S. Saraiva, N.L. Dias Filho, C.D. Nunes, P.D. Vaz, T.G. Nunes, M.J. Calhorda, *Micropor. Mesopor. Mater.* 117 (2009) 670–677.
- [15] M.S. Saraiva, C.D. Nunes, T.G. Nunes, M.J. Calhorda, *J. Mol. Catal. A* 321 (2010) 92–100.
- [16] P.K. Baker, M.B. Hursthouse, A.I. Karaulov, A.J. Lavery, K.M.A. Malik, D.J. Muldoon, A. Shawcross, *J. Chem. Soc. Dalton Trans.* (1994) 3493–3498.
- [17] M. Vasconcellos-Dias, S.R.M.M. de Aguiar, C.D. Nunes, P.D. Vaz, T.G. Nunes, M.J. Calhorda, *Curr. Inorg. Chem.* 1 (2011) 146–155.
- [18] (a) J.-M. Brégeault, *Dalton Trans.* (2003) 3289–3302; (b) K.A. Jørgensen, *Chem. Rev.* 89 (1989) 431–458.
- [19] F.E. Kühn, M. Groarke, É. Bencze, E. Herdtweck, A. Prazeres, A.M. Santos, M.J. Calhorda, C.C. Romão, I.S. Gonçalves, A.D. Lopes, M. Pillinger, *Chem. Eur. J.* 8 (2002) 2370–2383.
- [20] A. Al-Ajlouni, D. Veljanovski, A. Capapé, J. Zhao, E. Herdtweck, M.J. Calhorda, F.E. Kühn, *Organometallics* 28 (2009) 639–645.
- [21] J.C. Alonso, P. Neves, M.J. Pires da Silva, S. Quintal, P.D. Vaz, C. Silva, A.A. Valente, P. Ferreira, M.J. Calhorda, V. Félix, M.G.B. Drew, *Organometallics* 26 (2007) 5548–5556.
- [22] (a) Y. Yamaguchi, K. Ogata, K. Kobayashi, T. Ito, *Dalton Trans.* (2004) 3982–3990; (b) P.K. Baker, *Adv. Organomet. Chem.* 40 (1996) 45–115.
- [23] (a) B.M. Trost, M. Lautens, *J. Am. Chem. Soc.* 104 (1982) 5543–5545; (b) B.M. Trost, M. Lautens, *J. Am. Chem. Soc.* 109 (1987) 1469–1478; (c) B.M. Trost, C.A. Merlic, *J. Am. Chem. Soc.* 112 (1990) 9590–9600.
- [24] D. Morales, J. Pérez, L. Riera, V. Riera, R. Corzo-Suárez, S. García-Granda, D. Miguel, *Organometallics* 21 (2002) 1540–1545.
- [25] V.S. Joshi, M. Nandi, H. Zhang, B.S. Haggerty, A. Sarkar, *Inorg. Chem.* 32 (1993) 1301–1303.
- [26] A. Sakthivel, J. Zhao, G. Raudaschl-Sieber, M. Hanzlik, A.S.T. Chiang, F.E. Kühn, *Appl. Catal. A Gen.* 281 (2005) 267–273.
- [27] A.J. Burke, *Coord. Chem. Rev.* 252 (2008) 170–175.
- [28] N.L.D. Filho, F.C.M. Portugal, J.M.F. Nogueira, P. Brandão, V. Félix, P.D. Vaz, C.D. Nunes, M.J. Calhorda, *Organometallics* 31 (2012) 4495–4503.
- [29] J.L. Walter, H. Freiser, *Anal. Chem.* 25 (1953) 127–130.
- [30] J.L. Walter, H. Freiser, *Anal. Chem.* 26 (1954) 217–221.
- [31] W.D. Johnston, H. Freiser, *Anal. Chim. Acta* 11 (1954) 301–308.
- [32] M.J. Calhorda, A.R. Dias, *J. Chem. Soc. Dalton Trans.* (1980) 1443–1447.
- [33] M. Vasconcellos-Dias, C.D. Nunes, P.D. Vaz, P. Ferreira, M.J. Calhorda, *Eur. J. Inorg. Chem.* (2007) 2917–2925.
- [34] M.S. Saraiva, C.D. Nunes, T.G. Nunes, M.J. Calhorda, *Appl. Catal. A Gen.* 455 (2013) 172–182.
- [35] C.D. Nunes, M. Pillinger, A.A. Valente, J. Rocha, A.D. Lopes, I.S. Gonçalves, *Chem. Eur. J.* (2003) 3870–3877.
- [36] B. Marler, U. Oberhagemann, S. Voltmann, H. Gies, *Micropor. Mater.* 6 (1996) 375–383.
- [37] W. Hammond, E. Prouzet, S.D. Mahanti, T.J. Pinnavaia, *Micropor. Mesopor. Mater.* 27 (1999) 19–25.
- [38] S.J. Gregg, K.S.W. Sing, *Adsorption, Surface Area and Porosity*, second ed., Academic Press, London, 1982.
- [39] M.D. Alba, A. Becerro, J. Klinowski, *J. Chem. Soc. Faraday Trans.* 92 (1996) 849–854.
- [40] A.A. Romero, M.D. Alba, W. Zhou, J. Klinowski, *J. Phys. Chem. B* 101 (1997) 5294–5300.
- [41] M. Kruk, M. Jaroniec, *Langmuir* 15 (1999) 5410–5413.
- [42] P. Ferreira, C.D. Nunes, P.D. Vaz, N. Bion, P. Brandão, J. Rocha, *Prog. Solid State Chem.* 33 (2005) 163–170.
- [43] C.I. Fernandes, N.U. Silva, P.D. Vaz, T.G. Nunes, C.D. Nunes, *Appl. Catal. A Gen.* 384 (2010) 84–93.
- [44] S.R. Hartmann, E.L. Hahn, *Phys. Rev.* 128 (1962) 2042–2053.
- [45] M. Kruk, M. Jaroniec, *Langmuir* 13 (1997) 6267–6273.
- [46] M. Kruk, V. Antochshuk, M. Jaroniec, *J. Phys. Chem. B* 103 (1999) 10670–10683.
- [47] W.D. Harkins, G. Jura, *J. Am. Chem. Soc.* 66 (1944) 919–927.
- [48] W.D. Harkins, G. Jura, *J. Am. Chem. Soc.* 66 (1944) 1362–1366.